

SSPINNpose: A Self-Supervised PINN for Inertial Pose and Dynamics Estimation

Markus Gambietz¹, Eva Dorschky², Altan Akat², Marcel Schöckel², Jörg Miehl³, and Anne D. Koelewijn¹

¹Chair of Autonomous Systems and Mechatronics, FAU
Erlangen-Nürnberg, Erlangen, Germany

²Machine Learning and Data Analytics Lab, FAU
Erlangen-Nürnberg, Erlangen, Germany

³Engineering Design, FAU Erlangen-Nürnberg, Erlangen,
Germany

Abstract

Accurate real-time estimation of human movement dynamics, including internal joint moments and muscle forces, is essential for applications in clinical diagnostics and sports performance monitoring. Inertial measurement units (IMUs) provide a minimally intrusive solution for capturing motion data, particularly when used in sparse sensor configurations. However, current real-time methods rely on supervised learning, where a ground truth dataset needs to be measured with laboratory measurement systems, such as optical motion capture. These systems are known to introduce measurement and processing errors and often fail to generalize to real-world or previously unseen movements, necessitating new data collection efforts that are time-consuming and impractical. To overcome these limitations, we propose SSPINNpose, a self-supervised, physics-informed neural network that estimates joint kinematics and kinetics directly from IMU data, without requiring ground truth labels for training. We run the network output through a physics model of the human body to optimize physical plausibility and generate virtual measurement data.

Using this virtual sensor data, the network is trained directly on the measured sensor data instead of a ground truth. When compared to optical motion capture, SSPINNpose is able to accurately estimate joint angles and joint moments at an RMSD of 8.7° and 4.9 BWBH%, respectively, for walking and running at speeds up to 4.9 m s^{-1} at a latency of 3.5 ms. Furthermore, the framework demonstrates robustness across sparse sensor configurations and can infer the anatomical locations of the sensors. These results underscore the potential of SSPINNpose as a scalable and adaptable solution for real-time biomechanical analysis in both laboratory and field environments.

1 Introduction

Understanding the injury mechanisms important for their prevention. However, injuries seldomly occur in controlled environments [1, 2]. Therefore, in-the-wild capturing of human movement dynamics, e.g. kinematics, joint torques, and ground reaction forces (GRFs), is required. Currently, the gold standard for capturing kinematics is optical motion capture (OMC), which is limited to a lab environment. In OMC, a person is fitted with reflective markers that are tracked by multiple cameras. Joint torques are estimated from the kinematics and force data, which are measured using force plates embedded into the floor, which further limits the environment. Applying the markers by hand is error-prone and the resulting kinematics can vary between different assessors and laboratories [3, 4]. Furthermore, different processing techniques can also lead to different results [5].

An alternative to OMC is the use of inertial measurement units (IMUs). These small, lightweight sensors can be worn during sports activities. Recent studies have explored methods that, based on inertial sensing, estimate poses [6, 7, 8, 9, 10, 11], forces [12] or full dynamics [13, 14, 15, 16, 17, 18]. The dynamics estimations are either based on deep learning [6, 18, 15], trajectory optimization [14, 17] or static optimization [13]. Current deep learning methods rely on supervised learning, which requires labeled data for training and, therefore, inherit the limitations and biases [4] of OMC. As a practical example, motions like high-speed running or sprinting require a large recording area, and are absent in widely used public IMU datasets like DIP-IMU and TotalCapture [9, 19]. Additionally, these datasets do not include force data. On the other hand, optimization-based methods need no labeled data but are computationally expensive, therefore not capable of real-time inference. This

furthermore makes them infeasible for analyzing dynamics over a long time period, which, for example, could be a running session leading to an injury. Both deep learning and optimization-based methods can handle sparse IMU configurations [18, 6, 17, 20], where not every body part is equipped with an IMU. This can make a system more practical for the user, but also makes the reconstruction of human movement dynamics even more challenging [8]. Similar to optical markers, the placement of IMUs can introduce errors in the kinematics estimation. Therefore, inferring the sensor placement from the data can be highly beneficial.

To address these limitations, we introduce SSPINNpose, which combines the real-time inference of learning-based methods with the ability of optimization-based approaches to reconstruct motions without relying on labeled data. The core principle behind SSPINNpose, a self-supervised physics-informed learning method, is that if an estimated motion is physically correct and corresponds to the measured IMU data, it is likely to be the correct motion. During training, the network is therefore guided to generate physically plausible motions that align with IMU data through virtual sensors. We further exploit auxiliary assumptions to accelerate training, mitigate local minima or enforce known properties of human movement. Our main contribution is to transform the trajectory optimization problems from Li et al. [17] and Dorschky et al. [14] into a self-supervised learning problem, which allows for real-time inference. We further demonstrate that our method can be used with sparse IMU configurations and to estimate the IMU placement. To our knowledge, SSPINNpose is the first real-time method for estimating biomechanical variables from inertial sensor data without labeled training data.

2 Related Work

Our work focuses on gait analysis, specifically the estimation of human movement dynamics, including both kinematics and the internal/external forces acting on the body. Since most dynamic motion during straight walking or running occurs in the lower limbs, particularly in the sagittal (forward-upward) plane, we review works that either examine full-body motion or focus on this plane.

Deep learning for movement dynamics: In order to estimate the 3D pose of a person in real-time from sparse IMU configurations, Huang et al. [9] proposed a deep learning-based method using a recurrent neural network (RNN). Subsequent work enhanced motion accuracy and allowed for flexible sensor configurations [6, 7, 10, 21]. Since visually plausible motion was prioritized in these early methods, physical correctness, such as accurate force estimation, became a significant next step. Therefore, Winkler et al. [18] trained reinforcement learning agents to control torque-driven multibody dynamics models in a physical simulator. Another approach, Physical Inertial Poser (PIP), [16] introduced a physics module to create physically plausible motions. The physics module contains a proportional-derivative (PD) controller and a motion optimizer, which also yields joint torques and GRFs, but only the kinematics have been validated so far. Similar to PIP, two-stage inference methods, where kinematics are first estimated with a learned prior and then dynamically updated with a physics model, are established in the domain of video-based pose estimation [22, 23, 24, 25, 26].

In biomechanical applications, reference data was often recorded with OMC in combination with force plates, from which joint angles and torques can be estimated via inverse kinematics and inverse dynamics. Supervised deep learning models have demonstrated to accurately predict these outcome variables from IMU data in a single inference step. Examples span a range of applications, such as gait analysis [27, 28, 15], slopes and stair climbing [29], activities of daily living [30] or pediatric care [31].

All deep learning-based inertial pose and dynamics estimation methods to date rely on labeled data for training. Therefore, these methods are unable to predict out-of-distribution movements. Furthermore, supervised methods inherit limitations from the reference system that was used for labelling, which is usually OMC, such as systemic and processing biases [4] or confinement to laboratory spaces. Our method requires no labeled data for training as we use a fully self-supervised approach.

Optimization-based movement dynamics: To estimate movement dynamics without labeled data, one can use optimization-based methods. Based on kinematics estimated by the inertial motion capture system Xsens, Karatsidis et al- [13] were first to propose the use of inverse methods to estimate GRFs and joint torques. From the estimated kinematics, they used static optimization to find the GRF, and then used inverse dynamics to estimate

the joint torques. They modeled the human body as a 3D musculoskeletal model with 39 degrees of freedom. However, their method has not been validated on running data and is not capable of handling sparse IMU setups or real-time inference. Furthermore, errors can accumulate during the multiple processing steps.

Movement dynamics can also be estimated in a single step with a trajectory optimization by finding control inputs, e.g. torques, for a simulation that best fits the IMU data. A solution to this can be found by solving an optimal control problem. In optimal control, an objective function, in this case the difference between the actual and simulated IMU data, is minimized while satisfying dynamics constraints imposed by a multibody dynamics model. Dorsky et al. [14] solved the resulting optimization problem with a two-dimensional musculoskeletal model with 9 degrees of freedom and 7 IMUs using a direct collocation method. However, they assumed the gait to be symmetric and periodic. Furthermore, they only optimized on averaged gait cycles data from multiple trials, while inference took more than 30 minutes for a single gait cycle. They later followed up with a study on sparse IMU configurations under the same settings [20]. Optimal control problems with sparse IMU configurations under no symmetry assumptions have been solved by Li et al. [17], but they relied on the detection of gait events instead. Detecting gait events from IMU data is an additional error source and unreliable for fast motions. 3D optimal control problems based on IMU data have not been solved yet, except when synthetic IMU data was used [32].

Our method is conceptually related to optimal control, as we aim to find a motion that minimizes the distance between actual and simulated IMU data and is physically plausible. Unlike optimal control, we create a surrogate model to stochastically map inputs to outputs instead of solving discrete optimization problems. A further difference is that optimal control problems use physical correctness as a constraint, while we use it as an optimization objective instead. This is similar to the solving strategy of constraint relaxation in optimization. As our method relies on stochastic optimization through a deep learning model, we use first-order solvers, such as Adam [33], instead of second-order solvers that are commonly used in optimal control problems, such as IPOPT [34]. Our method is advantageous in terms of pre-processing, as we do not need to detect gait events [17] or extract gait cycles under the assumption that these are periodic [14].

From optimization problems to self-supervised learning: Our work is based on the idea of transforming an optimization problem into a self-supervised learning problem. This paradigm leads to increased simulation speed, while not requiring labeled data and has been used in various fields. For example, for 3D human [35] and hand [36] shape matching, the shape of a hand or human body was predicted from a single image with a neural network. The shape, was then (neurally) rendered and compared to the input image. As the rendering process is differentiable, they can backpropagate the error to the neural network. A similar approach was used for the design of RF pulses in MRI [37], where an optimal RF pulse prior was learned via MRI simulations. Self-supervised learning is also used in cloth simulation, where the neural network predicts the mechanics of clothing during movement, which is then evaluated based on physical plausibility [38, 39]. In SSPINNpose, we reconstruct our input signal, comparable to Wan et al. [36], and aim for physical plausibility as in Santesteban et al. [39].

3 Method

3.1 Problem Formulation

Our goal is to reconstruct lower body movement dynamics in the sagittal plane using IMUs. We aim to train a neural network for this task in a fully self-supervised manner, meaning that no labeled data for the outputs will be available during training.

The input consists of sequential two-dimensional accelerometer and gyroscope measurements from up to seven IMUs placed on the feet, shanks, thighs, and pelvis, alongside parameters that define the multibody dynamics model (Fig. 1). The outputs are the generalized coordinates, joint torques and GRFs. All outputs are directly estimated by the neural network, except for the GRFs, which are estimated with a ground contact model based on the kinematics output.

3.2 SSPINNpose

We introduce SSPINNpose, a self-supervised physics-informed neural network designed to learn human movement dynamics from IMU data without labels. The term "physics-informed" refers to the integration of Kane's equa-

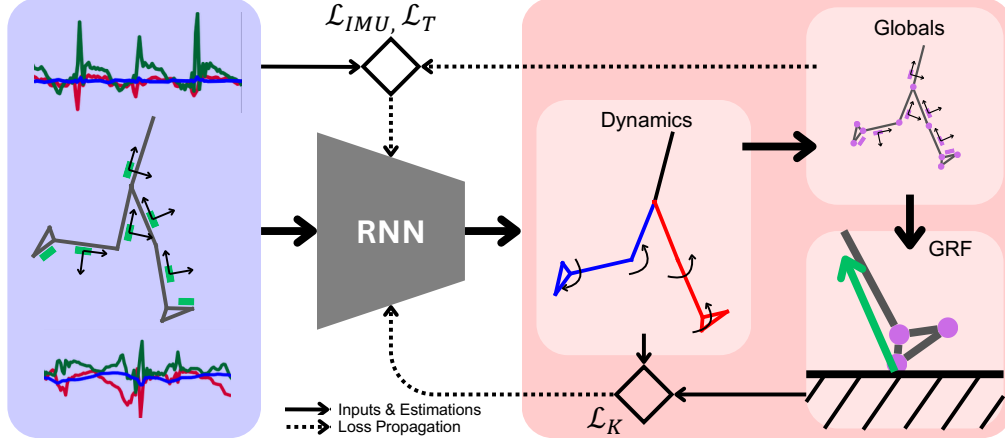


Figure 1: Overview of the SSPINNpose’s training scheme. The blue box shows inertial measure unit (IMU) signals from an unknown motion. For simplicity, we only show a single pose (gray). IMUs are annotated in light green. The RNN estimates the multibody dynamics in the first light red box. We then calculate the global kinematics for all joints, virtual IMUs, the heels and the toes (magenta). The ground reaction force (GRF, green) is then estimated based on the global ankle kinematics. Then we calculate the IMU loss (\mathcal{L}_{IMU}) and the temporal consistency loss (\mathcal{L}_T) based on the global positions and Kane’s Loss (\mathcal{L}_K) based on the estimated joint angles, torques and GRFs.

tions [40] and a temporal consistency loss. Kane’s equations ensure physical plausibility for all system states at each discretization point, while the temporal consistency loss ensures that the estimated velocities and accelerations align with changes in position and velocity over time. The self-supervised aspect relates to the reconstruction of the IMU data, allowing the model to learn from the inherent structure of the input signals. To ensure stable and fast training, we introduce further auxiliary losses that are based on either common assumptions in human movement or known properties of inertial sensors. In summary, SSPINNpose is trained with a weighted combination of the core (section 3.2.2) and auxiliary losses (section 3.2.3, see appendix A

for more details):

$$\mathcal{L} = \sum_{i \in \{IMU, T, K, GC\}} \lambda_i \mathcal{L}_i + \sum_{j \in \{B, \tau, slide, FS\}} \lambda_j \mathcal{L}_j. \quad (1)$$

3.2.1 RNN implementation

To capture the temporal dependencies inherent in human movements and inertial sensor data, we employ a recurrent neural network (RNN). We tested a LSTM [41] for real-time inference and a bidirectional LSTM that has access to future information, each followed by two dense layers to calculate the output. The network architecture is adapted from PIP [16]. At each time step t , the model receives the current IMU reading \mathbf{x}_t , body constants $\boldsymbol{\theta}_b$, IMU placement and rotations relative to their segment roots $\boldsymbol{\theta}_{IMU}$, and ground contact model parameters $\boldsymbol{\theta}_{gc}$. The input IMU data consists of 2D acceleration and 1D angular velocity data per sensor in the sagittal plane, and is augmented with Gaussian noise with a standard deviation of $\eta_{imu}\sigma(\mathbf{x}_i)$ for each input channel i , where η_{imu} is set to 0.25

The 46 output features $\hat{\mathbf{y}}_t$ consist of each 9 estimated generalized coordinates \mathbf{q} , velocities $\dot{\mathbf{q}}$, and accelerations $\ddot{\mathbf{q}}$, 6 torques $\boldsymbol{\tau}$ and 14 ground contact model states, which consists of the global kinematics of the ankle joint $\tilde{\mathbf{q}}_{ankle}$, $\tilde{\dot{\mathbf{q}}}_{ankle}$, and a current friction factor for each foot $\hat{\boldsymbol{\mu}}$. The horizontal root position is ambiguous, therefore we replace it by the integrated horizontal root velocity.

For the loss calculations introduced in the following sections, we compute the global kinematics for the joints \mathbf{p}_j , IMUs \mathbf{p}_{IMU} and ground contact points \mathbf{p}_{gc} based on the kinematics of the respective parent joint. The global kinematics of each point consist of its global position, x, y , and angle, α , as well as their first and second derivatives $\mathbf{p} = \{x, \dot{x}, \ddot{x}, y, \dot{y}, \ddot{y}, \alpha, \dot{\alpha}, \ddot{\alpha}\}$ (see appendix A for further details).

3.2.2 Physics Information and Self-Supervision

The main idea behind SSPINNpose is that a motion that is physically plausible and consistent with the IMU data is likely to be the correct motion. We enforce this by the following loss functions: Kane’s loss (\mathcal{L}_K), temporal consistency loss (\mathcal{L}_T) and IMU reconstruction loss (\mathcal{L}_{IMU}). These core components of SSPINNpose are illustrated in Figure 1.

Multibody Dynamics Model & Kane’s Equations: Our multibody dynamics model is a sagittal-plane lower limb model with 2 translational and 7 rotational degrees of freedom, which correspond to the generalized coordinates. The body consists of 7 segments: one trunk, and a thigh, shank, and foot for each leg. The body constants θ_b contain the mass, length, center of mass and moment of inertia for each segment. The body constants are linearly scaled based on the participant’s height [42]. We normalize all forces to bodyweight.

Using this dynamics model, we calculate the equations of motion based on Kane’s method [40], implemented in SymPy [43]. Kane’s formulation is advantageous for deep learning as it is the method that requires fewer equations to be solved to describe movement dynamics. Kane defined that the sum of internal (F_r^*) and external (F_r) forces acting on a system is zero. Therefore, we can define a loss term that enforces the physical plausibility of each estimated state:

$$\mathcal{L}_K = (|\mathbf{F}_r^* + \mathbf{F}_r|)^2 = f(\hat{\mathbf{y}}, \theta_b, \mathbf{F}_{gc})^2. \quad (2)$$

To estimate the GRF \mathbf{F}_{gc} , we model the foot-ground contact with a sliding contact point. The contact point’s position between the heel and toe is determined based on the global ankle rotation. The vertical component of the GRF is modeled as a linear spring-damper system as in [44], while the horizontal component is modeled as a friction cone with a learned current friction coefficient $\hat{\mu}$. To disentangle the GRF from the kinematics, we estimate the global ankle kinematics separately, which is supervised by the difference with the estimated forward kinematics (\mathcal{L}_{GC}) of the ankle. For more details, see appendix A.

Temporal Consistency Loss: While Kane’s method enforces physical plausibility at each time point, we also ensure that the derivatives of the estimated coordinates match the estimated velocities, and that the derivatives of the estimated velocities match the estimated accelerations. This loss is applied to the generalized coordinates \mathbf{q} . We normalize the loss by the standard deviation of the estimated coordinates or velocities over the sequence to ensure scale-invariance:

$$\mathcal{L}_T = \left(\frac{1}{2n_q} \sum_{i=1}^{n_q} \left(\left(\frac{d\mathbf{q}_i}{dt} - \dot{\mathbf{q}}_i \right) \sigma(\mathbf{q}_i)^{-1} + \left(\frac{d\dot{\mathbf{q}}_i}{dt} - \ddot{\mathbf{q}}_i \right) \sigma(\dot{\mathbf{q}}_i)^{-1} \right) \right)^2. \quad (3)$$

We chose this approximate integration method to decouple the learning of kinematics from movement dynamics, as numerical differentiation of the kinematics would cause exploding gradients in Kane’s equations.

IMU Reconstruction Loss: We obtain virtual IMU signals $\hat{\mathbf{x}}_{imu}$ [14] by rotating the kinematics of each IMU \mathbf{p}_{IMU} into its respective local coordinate system. These virtual IMU signals are then compared to the recorded IMU signals. We normalize the loss by the standard deviation over a sequence of the IMU signals per channel and the number of IMUs n_{imu} :

$$\mathcal{L}_{IMU} = \left(\frac{1}{n_{imu}} \sum_{i=1}^{n_{imu}} (\mathbf{x}_{imu} - \hat{\mathbf{x}}_{imu}) \sigma(\mathbf{x}_{imu})^{-1} \right)^2. \quad (4)$$

3.2.3 Auxiliary Losses

This section describes the auxiliary losses that we use to accelerate training, mitigate local minima or enforce known properties of human movement. For more details and an ablation study to justify these losses, refer to the appendix sections A and C.

Joint Limit and Ground Contact Force Bounds (\mathcal{L}_B): We penalize the model for exceeding joint limits and for violating bounds on maximum velocity and vertical position (see appendix A). Additionally, we assume that for each sequence, each foot supports at least 20% of the body weight. In practice, this avoids local minima where the model does not predict any ground contact or skips on one foot.

Torque Minimization (\mathcal{L}_τ): We apply a small weight on speed-weighted torque minimization, as minimizing effort is a common assumption in human movement and usually leads to more natural motions [44]. Similar to [14], we normalize the torques by the maximum speed of the root translation in the sagittal plane. As our training data might contain some non-movement phases, the speed normalization only applies to sequences with estimated moving speeds greater than 1 m s^{-1} .

Sliding Penalty (\mathcal{L}_{slide}): To prevent foot sliding when a ground reaction force (GRF) is present, we define sliding as the product of foot-ground speed

and vertical GRF. This formulation ensures that at least one of these variables is constrained to be zero.

Foot Speed (\mathcal{L}_{FS}): To speed up the training process and make our model less susceptible to local minima, we make use of known properties of foot-worn IMUs by reconstructing their global velocities ($\dot{\mathbf{p}}_{K,x}$) using a Kalman filter with zero-velocity updates [45, 46], as implemented in [47]. In practice, this term contributes to avoiding local minima. The IMU trajectory reconstruction algorithm is based on integration of the IMU signals which accumulates errors from drift and noise. Furthermore, zero-velocity updates are unreliable during running. As a consequence, we treat these reconstructed speeds as erroneous and only apply a penalty when the estimated foot-worn IMU speed from our kinematics differs by more than 30% from its reconstructed maximum speed during the sequence.

4 Experiments

In this section, we first describe the dataset used for training and evaluation, followed by the evaluation metrics used to assess our model’s performance. Next, we show and discuss model’s capability to estimate human movement dynamics from IMU data in section 4.1. We then showcase that our model can be finetuned for more accurate force estimation and that, by optimizing our input variables, SSPINNpose is capable of estimating the IMU placement (section 4.2). Finally, results and discussions on sparse IMU configurations (section 4.3) are shown.

Dataset We use the ”Lower-body Inertial Sensor and Optical Motion Capture Recordings of Walking and Running” dataset for training and evaluation [48]. The dataset contains data of persons walking and running through an area equipped with OMC cameras and a single force plate, along with continuous IMU signals. For every trial, the OMC data contains roughly 5 m of kinematics data and force plate data for a single step. We estimate the total running distance for the highest speed at ca. 20 m based on SSPINNposes output. We downsampled the IMU signals to 100 Hz. The dataset includes data from 10 participants, each performing 10 trials at 6 different speeds, ranging from 0.9 m s^{-1} to 4.9 m s^{-1} . For each condition, IMU data from the

first 7 trials were designated for training, while the remaining 3 were used for evaluation.

We selected the training data by applying a heuristic that identifies standing and turning phases based on the foot and pelvis IMU signals, respectively. This was done to include the run-up to the motion capture area and some steps after the motion capture area in our training set, while avoiding turning phases that we cannot reconstruct with a two-dimensional model. In total, our training data consists of 76 minutes of unlabeled IMU data. We processed the OMC and force plate data with addBiomechanics [5] to compare the resulting joint angles and joint torques. The first participant was excluded from addBiomechanics because of erroneous force plate readings. During training, we randomly selected sequences of 256 time steps from the training data, while full sequences were used during evaluation. Typical sequences from the datasets are visualized in appendix Figure 6. This dataset has been used by several other works focussing on sagittal-plane lower limb dynamics [14, 15, 20].

Metrics: We use the following metrics to evaluate our model: 1.) *Joint Angle Error (JAE)*: The root mean square deviation (RMSD) between the estimated joint angles and those obtained from addBiomechanics, including the root orientation, in degrees. 2.) *Joint Torque Error (JTE)*: The RMSD between the estimated joint torques and those obtained from addBiomechanics, in bodyweight-bodyheight percent (BWBH%). 3.) *GRF Error (GRFE)*: The root mean square error (RMSE) between the estimated GRFs and those obtained from the force plate, normalized by the bodyweight, in bodyweight percent (BW%). The GRF is the only outcome variable that can be directly measured, therefore, we consider it to be an error and not a deviation to a reference system. 4.) *Speed Error*: The RMSD between the estimated average speed and the sagittal-plane speed of the pelvis markers while the participant was crossing the OMC area, in m s^{-1} . For all metrics, lower values are better. We show an evaluation on metrics that are commonly used in computer graphics in the appendix B.

4.1 Quantitative and Qualitative Evaluation

SSPINNPOSE was able to predict joint angles, joint moments, ground reaction forces, and speed with similar accuracy when using an LSTM and a Bi-LSTM (Table 1). We evaluated SSPINNpose’s performance on continuous

Table 1: Quantitative comparison on continuous IMU data and on the test set of [14]. To compare against [14], we retrained and evaluated SSPINNpose in settings that are comparable to their methods. The metrics are defined in section 4.

Model	JAE [deg]	JTE [BWBH%]	GRFE [BW%]	Speed [m s ⁻¹]	No labels needed	Latency
SSPINNpose (LSTM)	8.7	4.9	16.4	0.19	✓	3.5 ms
SSPINNpose (Bi-LSTM)	8.9	5.0	18.8	0.15	✓	3.5 ms
CNN-based regression [15]	4.9	1.4	10.7	-	✗	<1 ms*
SSPINNpose (OCP)	8.9	6.8	23.8	0.25	✓	3.5 ms
Optimal Control [14]	6.3	2.6	17.9	0.25	✓	50 min

*needs to wait for a full gait cycle to complete before inference.

IMU data using a LSTM and a Bi-LSTM model, respectively. Between both, there are only minor differences in the outcome metrics. The LSTM model estimated dynamics and GRFs slightly more accurately, while the Bi-LSTM model estimated speed more accurately and produced smoother motions. The LSTM can estimate the joint angles and torques in real-time, with a latency of 3.5 ms. Training took approximately 16 hours on a NVIDIA RTX 3080 GPU. To compare against state of the art methods that report results on the same dataset, we show versions of our model with adapted training and evaluation schemes. To compare to [14], which optimized on ensemble averaged gait cycles, we trained and evaluated SSPINNpose (OCP) on ensemble averaged gait cycles from all 60 trials. Here, the JTE, GRFE and speed error are slightly higher compared to training and evaluation on continuous data.

SSPINNpose’s kinematics estimations are on par with current real-time deep learning-based methods [16] (see appendix B for more details). Compared to existing biomechanically validated methods, SSPINNpose is able to estimate the dynamics of human movement from IMU data in real-time without the need for labeled data. We achieve a speed error that is 0.1 m s⁻¹ smaller the current optimal control-based state of the art [20] when trained on continuous IMU data. The JAE, JTE, and GRFE, on the other hand, are generally larger than in regression-based methods such as [15], when tested under the same conditions. However, the optimal control-based meth-

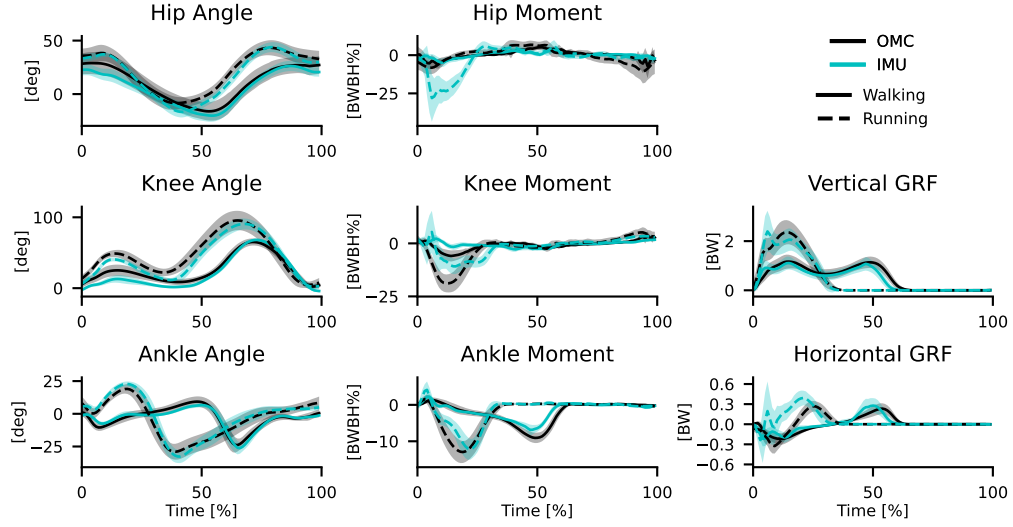


Figure 2: Average joint angles, torques and ground reaction forces (GRFs) for the right leg over all test gait cycles. Estimated with the Bi-LSTM. We segmented the gait cycles during which the force plate was hit and normalized them to a duration of 100 samples. Walking and running data is shown in solid and dashed lines, respectively. Our estimates are shown in cyan, the reference data is shown in black. The shaded area represents the standard deviation.

ods rely on assumptions that make them unusable for real-time inference by segmenting the data into gait cycles. Furthermore, they assumed the gait cycles to be symmetric and periodic, which limits the generalization towards arbitrary movements. The CNN-based regression method takes one gait cycle at a time as input, therefore introducing latency as gait cycles need to be completed before inference. We argue that inference on continuous IMU data is a more realistic scenario and therefore more relevant, while the need for gait cycle segmentation is a limitation of the other methods.

In Figure 2, we show the gait-cycle averages of the joint angles, torques and GRFs estimated with the Bi-LSTM model in comparison to the OMC reference. The kinematics were estimated accurately, with a small bias in the hip and knee angle. Especially in running, the hip and knee moment were not accurately estimated during the stance phase, which is the first 40 % of the gait cycle for running and the first 60 % for walking. The ankle moment and vertical GRF shows slightly lower values than the reference data, while the horizontal GRF could not be estimated correctly. SSPINNpose estimated the kinematics and speeds robustly, with median and 95th percentile errors of 5.2° and 16.7° for joint angles, and 3.1 % and 9.3 % for speed.

In SSPINNpose, the network implicitly learns the interconnection between movement kinematics and dynamics. In contrast, other real-time capable methods, such as [16, 22], use kinematical network output as an input signal for a PD controller and dynamics optimizer. Whether direct or two-stage inference is preferable depends on the application. Direct inference is faster and the dynamics are not subject to propagation errors from the kinematics. On the other hand, the two-stage inference can help with generalization towards unseen movements and can be more robust to noise. When testing SSPINNpose with PIP’s PD controller and optimizer, we found that the the PD controller hyperparameters needed to be adjusted. Depending on the hyperparameters, the PD controller could be used to slightly reduce the JTE while raising the JAE and smoothing the motion (see appendix C for implementation details).

Our method contains a number of assumptions and simplifications. As in [16], we assume that the ground is flat and the foot cannot slide. Information about the ground is present in the IMU data, and has been exposed in recent work by inferring terrain height maps [10]. It has yet to be shown whether the terrain information can also be learned without labels. The interaction between foot and ground is modeled as a linear spring-damper system. Furthermore, the multibody dynamics model is based on a generic

template, which is due to a lack of personalization options. As we fit towards IMU signals that are noisy, our model can learn to replicate that noise and becomes less physically plausible, which we are mitigating, but not eliminating by augmenting the input data with Gaussian noise. Our model is able to accurately estimate human movement dynamics despite these limitations, therefore we consider them to be an opportunity to make the estimations more accurate in the future.

4.2 Finetuning for Physics

Depending on the outcome variable of interest, we can finetune SSPINNpose by prioritizing different loss terms. In an ideal simulation, the estimated dynamics should perfectly match the actual motion. However, achieving a perfect simulation requires physical exactness, meaning that both Kane’s loss and the temporal consistency loss must be zero. Therefore, we finetuned the Bi-LSTM towards physics by increasing the weight of the Kane’s loss and the temporal consistency loss by a factor of 10. This reduced the JTE by 10% and the GRFE by 20%. However, as the IMU signals were not followed as strictly, the JAE increased by 5% and the speed error increased by 33%. After this finetuning, the biases in knee moment and vertical GRF were substantially reduced and only the bias in the hip torque during the stance phase in running remained. For use cases where the torques are of most interest, this trade-off should be acceptable.

A perfect simulation would require a correct multibody dynamics model with correct IMU positions. Our model and loss function can act together as a differential physical simulator. Therefore, we can optimize input parameters, including IMU orientations and positions. The IMU orientations and positions are prone to errors as they are placed and measured manually. Therefore, we finetuned the network and the IMU positions and orientations jointly for each participant. In Figure 3, we show the results of the IMU positioning optimization for all participants’ thigh IMUs. We use the trochanter and knee markers as reference for the hip and knee joints. We present the manually measured position of the thigh IMU in the dataset, which [48] assumed was located on the segment axis. We show that we are able to recover this misplacement from the dataset. For most participants, the position estimate is on or very close to the IMU housing. To our knowledge, current methods can only estimate the distance of an IMU from the joint center, but not the distance of the IMU to the segment axis [49]. This discrepancy

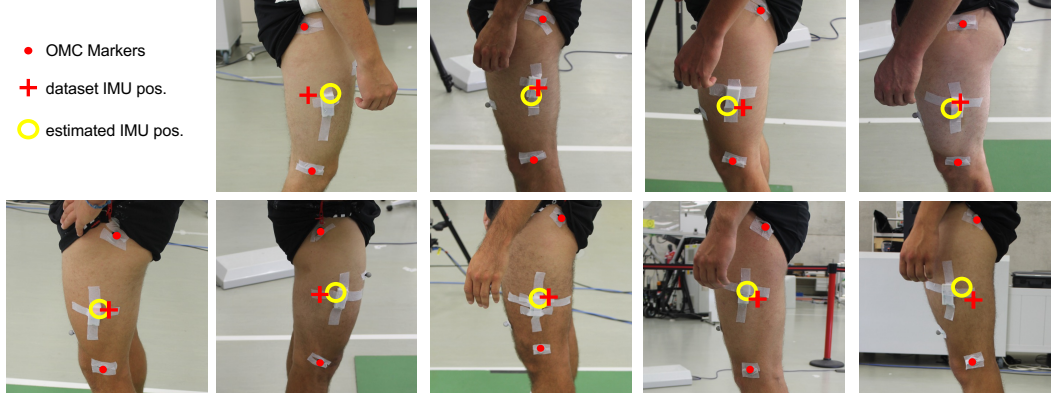


Figure 3: Comparison of IMU positionings from the dataset and our estimations. We use OMC markers as a reference frame. For all participants, we show either the right or left leg. We always chose the side where the IMU and OMC markers were clearly visible. If they were visible from both sides, we chose the picture that was taken more perpendicular to the sagittal plane.

between the positioning from the dataset and our estimation was only apparent for the thigh IMUs, and the margin of improvement in the metrics after personalization is very small (see appendix C). However, the personalization of the IMU positionings can make the model more robust to misplacements and misalignments when donning the IMUs.

There is no validation for the correctness of body constants and ground contact model parameters on the given dataset, as that would require medical imaging. Thus, we excluded these parameters from the IMU positioning optimization. However, when we optimized the body constants, we found that only the moments of inertia yielded unrealistic values, as they converged to zero. The convergence to zero is due to the formulation of Kane’s loss, which favours moments of inertia, as they lead to less force and therefore less physics error in general. For the body weight, the same issue would apply, but we mitigated that by optimizing for the weight distribution instead of the body weight itself.

4.3 Sparse IMU Configurations

In practice, the fewer IMUs one has to wear, the better. Therefore retrained the Bi-LSTM from scratch on configurations with only the foot-worn IMUs (F), foot and thigh IMUs (FT), and foot and pelvis IMUs (FP). Errors generally increased (Table 2), but the output motion is still physically and visually plausible (see appendix C). For the running motions in F and FT configurations, the ankle angle and therefore the origin of the GRF is visibly shifted. Between the configurations with and without a pelvis IMU, the trunk orientation is different for all motions. Therefore, there is likely a discrepancy between the actual, physically plausible, trunk orientation and the IMU orientation, i.e. the pelvis IMU might not be correctly aligned, which was also observed in [20]. Compared to [20], our increases in errors are similar for the F and FP configurations, but higher for the FT configuration. We believe our method is more affected by soft tissue artefacts, measurement errors caused by the movement of skin and muscle, from thigh IMUs compared to the optimal control method. As there is no hard constraint in SSPINNpose, it can trade off physical correctness for a better fit to the IMU signals, especially when they contain noise. On the other hand, hard constraints in optimal control do not allow physically incorrect motions. The pelvis and foot IMUs, however, are less affected by soft-tissue artefacts.

Table 2: Comparison of different sparse IMU configurations using the Bi-LSTM model on the evaluation metrics. The best results are shown in bold.

IMU configuration	JAE [deg]	JTE [BWBH%]	GRF [BW%]	Speed [m s ⁻¹]
All	8.9	5.0	18.8	0.15
Feet + Thighs	14.4	8.1	32.7	0.45
Feet + Pelvis	12.6	4.9	24.9	0.41
Feet	13.2	7.4	27.8	0.30

5 Conclusion

In this work, we presented SSPINNpose, a real-time method for the estimation of human movement dynamics from inertial sensor data that does

not require labeled training data. Instead, it relies on self-supervision and physics information to find plausible motions. We show that SSPINNpose can accurately estimate joint angles, torques, and GRFs from IMU data, while outperforming state-of-the-art methods in terms of horizontal speed estimation. Additionally, SSPINNpose effectively identifies movement patterns from sparse IMU configurations and personalizes IMU placement on the body. Given its capability to work with minimal IMU configurations and allow for personalization, SSPINNpose is a promising approach for long-term monitoring of athletes and understanding injury mechanisms.

There is room for more detailed modeling. For example, the model could be extended to 3D. As current 3D optimal control simulations have only been successfully solved for simulated IMU data, however, we are unsure whether SSPINNpose would be able to solve these tasks. To make the model even more detailed and biomechanically accurate, the torque actuators should be replaced with muscles. Furthermore, an unsupervised method for terrain mapping could be integrated. For supervised inertial pose estimation systems, this has already been shown to be possible [10]. Additionally, other data sources such as optical markers or radar could be tested.

Predictive simulations, an optimal control task where no reference data is given, are also of interest for future work. Concretely, the IMU tracking term would be replaced with a physiological movement objective, such as metabolic cost minimization. Here, self-supervised learning can be used to obtain a controller. The goal for SSPINNpose in this setting would be to be faster than model predictive control methods while being more accurate than reinforcement learning methods. Especially in muscle-driven simulations, the differentiable physics model is advantageous over reinforcement learning, as exploration for co-actuated systems is difficult [50].

In conclusion, SSPINNpose contributes to human movement analysis by providing a real-time method for the estimation of human movement dynamics from inertial sensor data without the need for labeled training data, which is crucial for movement analysis in the natural environment.

References

- [1] Kevin Wallbank, Carlie Ede, Glen Blenkinsop, and Sam Allen. Biceps Femoris Muscle States prior to and during a Hamstring Strain Injury

whilst Sprinting. In *ISBS Proceedings Archive*, volume 42: Iss 1, Article 193, Salzburg, 2024.

- [2] Bryan C. Heiderscheit, Dina M. Hoerth, Elizabeth S. Chumanov, Stephen C. Swanson, Brian J. Thelen, and Darryl G. Thelen. Identifying the time of occurrence of a hamstring strain injury during treadmill running: A case study. *Clinical Biomechanics*, 20(10):1072–1078, December 2005.
- [3] Jennifer L. McGinley, Richard Baker, Rory Wolfe, and Meg E. Morris. The reliability of three-dimensional kinematic gait measurements: A systematic review. *Gait & Posture*, 29(3):360–369, April 2009.
- [4] Sophie Fleischmann, Simon Dietz, Julian Shanbhag, Annika Wuensch, Marlies Nitschke, Jörg Miehl, Sandro Wartzack, Sigrid Leyendecker, Bjoern M. Eskofier, and Anne D. Koelewijn. Exploring Dataset Bias and Scaling Techniques in Multi-Source Gait Biomechanics: An Explainable Machine Learning Approach. *ACM Trans. Intell. Syst. Technol.*, 16(1):1–19, February 2025.
- [5] Keenon Werling, Michael Raitor, Jon Stingel, Jennifer L Hicks, Steve Collins, Scott Delp, and C Karen Liu. Rapid bilevel optimization to concurrently solve musculoskeletal scaling, marker registration, and inverse kinematic problems for human motion reconstruction. *bioRxiv*, pages 2022–08, 2022.
- [6] Xinyu Yi, Yuxiao Zhou, and Feng Xu. TransPose: Real-Time 3D Human Translation and Pose Estimation with Six Inertial Sensors. *ACM Trans. Graph.*, 40(4), July 2021.
- [7] Tom Van Wouwe, Seunghwan Lee, Antoine Falisse, Scott Delp, and C. Karen Liu. DiffusionPoser: Real-time Human Motion Reconstruction From Arbitrary Sparse Sensors Using Autoregressive Diffusion, March 2024.
- [8] Timo Von Marcard, Bodo Rosenhahn, Michael J Black, and Gerard Pons-Moll. Sparse inertial poser: Automatic 3d human pose estimation from sparse imus. In *Computer Graphics Forum*, volume 36, pages 349–360. Wiley Online Library, 2017.

- [9] Yinghao Huang, Manuel Kaufmann, Emre Aksan, Michael J. Black, Otmar Hilliges, and Gerard Pons-Moll. Deep Inertial Poser: Learning to Reconstruct Human Pose from Sparse Inertial Measurements in Real Time. *ACM Transactions on Graphics, (Proc. SIGGRAPH Asia)*, 37:185:1–185:15, November 2018.
- [10] Yifeng Jiang, Yuting Ye, Deepak Gopinath, Jungdam Won, Alexander W. Winkler, and C. Karen Liu. Transformer Inertial Poser: Real-Time Human Motion Reconstruction from Sparse IMUs with Simultaneous Terrain Generation. In *SIGGRAPH Asia 2022 Conference Papers*, SA '22, New York, NY, USA, 2022. Association for Computing Machinery.
- [11] Daniel Roetenberg, Henk Luinge, Per Slycke, et al. Xsens MVN: Full 6DOF human motion tracking using miniature inertial sensors. *Xsens Motion Technologies BV, Tech. Rep.*, 1:1–7, 2013.
- [12] Tian Tan, Peter B. Shull, Jenifer L. Hicks, Scott D. Uhlich, and Akshay S. Chaudhari. Self-Supervised Learning Improves Accuracy and Data Efficiency for IMU-Based Ground Reaction Force Estimation. *IEEE Trans. Biomed. Eng.*, 71(7):2095–2104, July 2024.
- [13] Angelos Karatsidis, Moonki Jung, H Martin Schepers, Giovanni Bellusci, Mark De Zee, Peter H Veltink, and Michael Skipper. Musculoskeletal model-based inverse dynamic analysis under ambulatory conditions using inertial motion capture. *Medical Engineering and Physics*, 65, 2019.
- [14] Eva Dorschky, Marlies Nitschke, Ann-Kristin Seifer, Antonie J. Van Den Bogert, and Bjoern M. Eskofier. Estimation of gait kinematics and kinetics from inertial sensor data using optimal control of musculoskeletal models. *Journal of Biomechanics*, 95:109278, October 2019.
- [15] Eva Dorschky, Marlies Nitschke, Christine F Martindale, Antonie J. van den Bogert, Anne D. Koelewijn, and Bjoern M. Eskofier. CNN-Based Estimation of Sagittal Plane Walking and Running Biomechanics From Measured and Simulated Inertial Sensor Data. *Frontiers in Bioengineering and Biotechnology*, 8(June):1–14, 2020.
- [16] Xinyu Yi, Yuxiao Zhou, Marc Habermann, Soshi Shimada, Vladislav Golyanik, Christian Theobalt, and Feng Xu. Physical Inertial Poser

- (PIP): Physics-aware Real-time Human Motion Tracking from Sparse Inertial Sensors. In *IEEE/CVF Conference on Computer Vision and Pattern Recognition (CVPR)*, June 2022.
- [17] Tong Li, Lei Wang, Jingang Yi, Qingguo Li, and Tao Liu. Reconstructing Walking Dynamics From Two Shank-Mounted Inertial Measurement Units. *IEEE/ASME Trans. Mechatron.*, 26(6):3040–3050, December 2021.
 - [18] Alexander Winkler, Jungdam Won, and Yuting Ye. QuestSim: Human Motion Tracking from Sparse Sensors with Simulated Avatars. In *SIGGRAPH Asia 2022 Conference Papers*, SA '22, New York, NY, USA, 2022. Association for Computing Machinery.
 - [19] Matt Trumble, Andrew Gilbert, Charles Malleson, Adrian Hilton, and John Collomosse. Total Capture: 3D Human Pose Estimation Fusing Video and Inertial Sensors. In *2017 British Machine Vision Conference (BMVC)*, 2017.
 - [20] Eva Dorschky, Marlies Nitschke, Matthias Mayer, Ive Weygers, Heiko Gassner, Thomas Seel, Bjoern M. Eskofier, and Anne D. Koelewijn. Comparing sparse inertial sensor setups for sagittal-plane walking and running reconstructions. *Front. Bioeng. Biotechnol.*, 13:1507162, February 2025.
 - [21] Yu Zhang, Songpengcheng Xia, Lei Chu, Jiarui Yang, Qi Wu, and Ling Pei. Dynamic Inertial Poser (DynaIP): Part-Based Motion Dynamics Learning for Enhanced Human Pose Estimation with Sparse Inertial Sensors, March 2024.
 - [22] Soshi Shimada, Vladislav Golyanik, Weipeng Xu, and Christian Theobalt. PhysCap: Physically Plausible Monocular 3D Motion Capture in Real Time, December 2020.
 - [23] Kevin Xie, Tingwu Wang, Umar Iqbal, Yunrong Guo, Sanja Fidler, and Florian Shkurti. Physics-based Human Motion Estimation and Synthesis from Videos, August 2022.
 - [24] Muhammed Kocabas, Ye Yuan, Pavlo Molchanov, Yunrong Guo, Michael J. Black, Otmar Hilliges, Jan Kautz, and Umar Iqbal. PACE:

Human and Camera Motion Estimation from in-the-wild Videos, October 2023.

- [25] Xinyu Yi, Yuxiao Zhou, Marc Habermann, Vladislav Golyanik, Shaohua Pan, Christian Theobalt, and Feng Xu. EgoLocate: Real-time Motion Capture, Localization, and Mapping with Sparse Body-mounted Sensors, May 2023.
- [26] Ye Yuan, Shih-En Wei, Tomas Simon, Kris Kitani, and Jason Saragih. SimPoE: Simulated Character Control for 3D Human Pose Estimation. In *2021 IEEE/CVF Conference on Computer Vision and Pattern Recognition (CVPR)*, pages 7155–7165, Nashville, TN, USA, June 2021. IEEE.
- [27] Hyerim Lim, Bumjoon Kim, and Sukyung Park. Prediction of Lower Limb Kinetics and Kinematics during Walking by a Single IMU on the Lower Back Using Machine Learning. *Sensors*, 20(1):130, December 2019.
- [28] Vincent Hernandez, Davood Dadkhah, Vahid Babakeshizadeh, and Dana Kulić. Lower body kinematics estimation from wearable sensors for walking and running: A deep learning approach. *Gait & Posture*, 83:185–193, January 2021.
- [29] Wei-Han Chen, Yin-Shin Lee, Ching-Jui Yang, Su-Yu Chang, Yo Shih, Jien-De Sui, Tian-Sheuan Chang, and Tzyy-Yuang Shiang. Determining motions with an IMU during level walking and slope and stair walking. *Journal of Sports Sciences*, 38(1):62–69, January 2020.
- [30] Fanjie Wang, Wenqi Liang, Hafiz Muhammad Rehan Afzal, Ao Fan, Wenjiong Li, Xiaoqian Dai, Shujuan Liu, Yiwei Hu, Zhili Li, and Pengfei Yang. Estimation of Lower Limb Joint Angles and Joint Moments during Different Locomotive Activities Using the Inertial Measurement Units and a Hybrid Deep Learning Model. *Sensors*, 23(22):9039, November 2023.
- [31] Shima Mohammadi Moghadam, Pablo Ortega Auriol, Ted Yeung, and Julie Choisne. 3D gait analysis in children using wearable sensors: Feasibility of predicting joint kinematics and kinetics with personalized machine learning models and inertial measurement units. *Front. Bioeng. Biotechnol.*, 12:1372669, March 2024.

- [32] Marlies Nitschke, Eva Dorschky, Sigrid Leyendecker, Bjoern M Eskofier, and Anne D Koelewijn. 3D kinematics and kinetics of change of direction motions reconstructed from virtual inertial sensor data through optimal control simulation, 2023.
- [33] Diederik P. Kingma and Jimmy Ba. Adam: A Method for Stochastic Optimization, January 2017.
- [34] Andreas Wächter and Lorenz T Biegler. On the implementation of an interior-point filter line-search algorithm for large-scale nonlinear programming. *Mathematical Programming*, 106(1):25–57, 2006.
- [35] Luca Schmidtke, Benjamin Hou, Athanasios Vlontzos, and Bernhard Kainz. Self-supervised 3D Human Pose Estimation in Static Video via Neural Rendering. In Leonid Karlinsky, Tomer Michaeli, and Ko Nishino, editors, *Computer Vision – ECCV 2022 Workshops*, volume 13803, pages 704–713. Springer Nature Switzerland, Cham, 2023.
- [36] Chengde Wan, Thomas Probst, Luc Van Gool, and Angela Yao. Self-Supervised 3D Hand Pose Estimation Through Training by Fitting. In *2019 IEEE/CVF Conference on Computer Vision and Pattern Recognition (CVPR)*, pages 10845–10854, Long Beach, CA, USA, June 2019. IEEE.
- [37] Albert Jang, Xingxin He, and Fang Liu. Physics-guided self-supervised learning: Demonstration for generalized RF pulse design. *Magnetic Resonance in Med*, page mrm.30307, October 2024.
- [38] Hugo Bertiche, Meysam Madadi, and Sergio Escalera. PBNS: Physically Based Neural Simulator for Unsupervised Garment Pose Space Deformation, May 2021.
- [39] Igor Santesteban, Miguel A. Otaduy, and Dan Casas. SNUG: Self-Supervised Neural Dynamic Garments, April 2022.
- [40] Thomas R. Kane and David A. Levinson. *Dynamics: Theory and Applications*. McGraw Hill Series in Mechanical Engineering. McGraw-Hill, New York, NY, 1985.
- [41] S Hochreiter. Long short-term memory. *Neural Computation MIT-Press*, 1997.

- [42] David A. Winter. *Biomechanics and Motor Control of Human Movement*. Wiley, Hoboken, N.J, 4th ed edition, 2009.
- [43] Aaron Meurer, Christopher P. Smith, Mateusz Paprocki, Ondřej Čertík, Sergey B. Kirpichev, Matthew Rocklin, AmiT Kumar, Sergiu Ivanov, Jason K. Moore, Sartaj Singh, Thilina Rathnayake, Sean Vig, Brian E. Granger, Richard P. Muller, Francesco Bonazzi, Harsh Gupta, Shivam Vats, Fredrik Johansson, Fabian Pedregosa, Matthew J. Curry, Andy R. Terrel, Štěpán Roučka, Ashutosh Saboo, Isuru Fernando, Sumith Kulal, Robert Cimrman, and Anthony Scopatz. SymPy: Symbolic computing in Python. *PeerJ Computer Science*, 3:e103, January 2017.
- [44] Antonie J. van den Bogert, Dimitra Blana, and Dieter Heinrich. Implicit methods for efficient musculoskeletal simulation and optimal control. *Procedia IUTAM*, 2(2011):297–316, January 2011.
- [45] Joan Solà. Quaternion kinematics for the error-state Kalman filter, November 2017.
- [46] David Simon Colomar, John-Olof Nilsson, and Peter Handel. Smoothing for ZUPT-aided INSs. In *2012 International Conference on Indoor Positioning and Indoor Navigation (IPIN)*, pages 1–5, Sydney, Australia, November 2012. IEEE.
- [47] Arne Küderle, Martin Ullrich, Nils Roth, Malte Ollenschläger, Alzhraa A. Ibrahim, Hamid Moradi, Robert Richer, Ann-Kristin Seifer, Matthias Zürl, Raul C. Șîmpetru, Liv Herzer, Dominik Prossel, Felix Kluge, and Bjoern M. Eskofier. Gaitmap—An Open Ecosystem for IMU-Based Human Gait Analysis and Algorithm Benchmarking. *IEEE Open J. Eng. Med. Biol.*, 5:163–172, 2024.
- [48] Eva Dorschky, Marlies Nitschke, Ann-Kristin Seifer, Antonie van den Bogert, Anne Koelewijn, and Bjoern Eskofier. Lower-body Inertial Sensor and Optical Motion Capture Recordings of Walking and Running, June 2024.
- [49] Thomas Seel, Jörg Raisch, and Thomas Schauer. IMU-Based Joint Angle Measurement for Gait Analysis. *Sensors*, 14(4):6891–6909, April 2014.

- [50] Pierre Schumacher, Daniel Häufle, Dieter Büchler, Syn Schmitt, and Georg Martius. DEP-RL: Embodied Exploration for Reinforcement Learning in Overactuated and Musculoskeletal Systems, April 2023.
- [51] Matthew Loper, Naureen Mahmood, Javier Romero, Gerard Pons-Moll, and Michael J. Black. SMPL: A Skinned Multi-Person Linear Model. *ACM Trans. Graph.*, 34(6), November 2015.

A Implementation Details

RNN & Hyperparameters: We use a network architecture similar to physics inertial poser (PIP) [16]. We use a LSTM with 2 layers with a hidden size of 256, while the output layers are of size 128 and 46, respectively. The LSTM has a dropout rate of 40 %. Further hyperparameters, including the weighting between the loss terms, are listed in table 3. We take the hyperparameters from PIP, as we use the same architecture. The loss weights were tuned manually.

Table 3: Hyperparameters in SSPINNpose.

Parameter	Value
learning rate	10^{-3}
optimizer	Adam
batch size	32
criterion	MSE
η_{imu}	0.25
λ_K	3.0
λ_T	3.0
λ_{IMU}	30.0
λ_{ankle}	100.0
λ_B	10000.0
λ_τ	1.0
λ_{slide}	30.0
λ_{FS}	1.0

Calculation of point kinematics: We list the equations to calculate the global kinematics, containing the positions (x, y) and angle α , of a point $\mathbf{p} = \{x, \dot{x}, \ddot{x}, y, \dot{y}, \ddot{y}, \alpha, \dot{\alpha}, \ddot{\alpha}\}$, based on its parent segment, here. For calculation, the parent is defined by an offset d_x, d_y , a point $\mathbf{p}' = \{x', \dot{x}', \ddot{x}', y', \dot{y}', \ddot{y}', \alpha', \dot{\alpha}', \ddot{\alpha}'\}$. First, $\{\alpha, \dot{\alpha}, \ddot{\alpha}\}$ are set by adding the local coordinates \mathbf{q}_p to \mathbf{p}' for the respective point. Then, $\{x, \dot{x}, \ddot{x}, y, \dot{y}, \ddot{y}\}$ are calculated as follows:

$$x = x' + \cos(\alpha')d_x - \sin(\alpha')d_y, \quad (5)$$

$$y = y' + \sin(\alpha')d_x + \cos(\alpha')d_y, \quad (6)$$

$$\dot{x} = \dot{x}' - (\sin(\alpha')d_x + \cos(\alpha')d_y) \dot{\alpha}', \quad (7)$$

$$\dot{y} = \dot{y}' + (-\sin(\alpha')d_y + \cos(\alpha')d_x) \dot{\alpha}', \quad (8)$$

$$\ddot{x} = \ddot{x}' + \left(-d_x \dot{\alpha}'^2 - \ddot{\alpha}' d_y\right) \cos \alpha' - \left(-d_y \dot{\alpha}'^2 + \ddot{\alpha}' d_x\right) \sin \alpha', \quad (9)$$

$$\ddot{y} = \ddot{y}' + \left(-d_x \dot{\alpha}'^2 - \ddot{\alpha}' d_y\right) \sin \alpha' + \left(-d_y \dot{\alpha}'^2 + \ddot{\alpha}' d_x\right) \cos \alpha'. \quad (10)$$

The global kinematics are only directly estimated for the pelvis and the ankle. Therefore, the global kinematics based on the pelvis are first calculated for the hip joint position and pelvis IMU and then propagated along the kinematic chain. From the ankle kinematics that are separately estimated, the heel and ankle point globals are calculated.

Ground contact model: We determine the ground contact point based on the global ankle rotation α_{ankle} , where the contact point is positioned on the line between heel and toe. The exact position is determined as $(\tanh(\alpha_{ankle} * 7) + 1)/2$, where 1 corresponds to the toe and 0 to the heel. The GRF is calculated as: $\mathbf{F}_y = -k\zeta(\beta \mathbf{p}_{gc,y})(1 - b\dot{\mathbf{p}}_{gc,y})/\beta$ with $\beta = 300$, stiffness $k = 100 \text{ BW/m}$, damping $b = 0.75 \text{ N s m}^{-1}$, and $\mathbf{F}_x = \mu_{max} \tanh(\hat{\mu}) \mathbf{F}_y$, with $\mu_{max} = 0.5$. The global ankle kinematics $\tilde{\mathbf{p}}_{ankle}$ are estimated separately and supervised by the estimated forward kinematics of the ankle \mathbf{p}_{ankle} :

$$\mathcal{L}_{GC} = \left(\frac{1}{n_{ankle}} \sum_{i=1}^{n_{ankle}} ((\tilde{\mathbf{p}}_{ankle} - \mathbf{p}_{ankle}) / \sigma(\mathbf{p}_{ankle})) \right)^2. \quad (11)$$

Bounds on joint limits and maximum velocity: For hip and ankle, we set the joint ranges to $[-\pi/3, \pi/3]$. As the knee can extend less, its joint range was set to $[-\pi/3, 0.1]$. The maximum velocity was set to $[-10 \text{ m s}^{-1}, 10 \text{ m s}^{-1}]$, while the vertical root position was set to $[0 \text{ m}, 2 \text{ m}]$.

Equations for the auxiliary losses: The torque minimization loss is calculated as:

$$\mathcal{L}_\tau = \left(\sum \tau / \max(\dot{\mathbf{p}}_{0,x}, 1) \right)^2, \quad (12)$$

where τ is the joint torque and $\dot{\mathbf{p}}_{0,x}$ is the speed of the root translation in the sagittal plane. The sliding penalty loss is calculated as:

$$\mathcal{L}_{slide} = \left(\frac{1}{n_{gc}} \sum_{i=1}^{n_{gc}} (|\dot{\mathbf{p}}_{gc,x}| \mathbf{F}_{gc,y}) \right)^2, \quad (13)$$

where $\dot{\mathbf{p}}_{gc,x}$ is the horizontal speed of the foot and $\mathbf{F}_{gc,y}$ is the vertical GRF. The foot speed loss is calculated as:

$$\mathcal{L}_{FS} = \left(\frac{1}{2} \sum_{\mathbf{p} \in \mathbf{p}_{ankle}} |\dot{\mathbf{p}}_x - \dot{\mathbf{p}}_{K,x}| - 0.3 \max(\dot{\mathbf{p}}_{K,x}) \right)^2, \quad (14)$$

where $\dot{\mathbf{p}}_{K,x}$ is the reconstructed horizontal speed of the foot-worn IMU and $\dot{\mathbf{p}}_x$ is the estimated horizontal speed of the foot-worn IMU.

B Comparison to 3D pose estimation

Current state-of-the-art 3D pose estimation methods are typically evaluated on different metrics than those that biomechanists are interested in, which are listed in table 4: 1.) *Jitter*: The third derivative of the joint positions in km s^{-3} . 2.) *Global Orientation Error (GOE)*: The mean absolute error (MAE) between estimated global segment orientations and those obtained from addBiomechanics, including the root orientation, in degrees. This term is similar to the SIP error, which measures the accuracy of global limb orientations in 3D. 3.) *Mean Absolute Joint Angle Error (JA-MAE)*: The MAE between estimated joint angles and those obtained from addBiomechanics, including the root orientation, in degrees. 4.) *Joint Positioning Error (JPE)*: The mean distance between the knee and ankle position in our estimation and the position of the respective OMC marker, in cm. The greater trochanter marker was aligned with the hip joint in our estimations.

Compared to PIP [16], our results show lower angular errors, slightly higher positioning errors and higher jitter. None of these metrics is directly comparable due to different reasons:

Table 4: The top half shows results of our baseline models on more additional metrics for walking and all movements. For comparison, results from PIP [16] are listed in the bottom half on its datasets.

SSPINNpose	Jitter	GOE	JA-MAE	JPE	Latency (ms)
	[km s^{-1}]	[deg]	[deg]	[cm]	[ms]
Walking	0.75	4.9	6.7	6.8	3.5
All motions	1.95	6.9	7.0	6.5	3.5
PIP (Dataset)		SIP			
		[deg]			
DIP-IMU	0.24	15.02	8.73	5.04	16
TotalCapture	0.20	12.93	12.04	6.51	16

- Different model configuration: SMPL [51] is a 3D model, which PIP used, that contains more joints and rotational degrees of freedom. Therefore, the rotational errors can be bigger, while the joint positions are closer to the reference data. The positioning of joints and their distances to the aligned root joint also influences the metrics. Jitter is affected similarly as JPE.
- Different evaluation method in JPE: In state-of-the-art methods, the reference joint centers are found by fitting SMPL to the reference data. On the other hand, we believe that the sagittal position of the knee and ankle markers is more precisely reflecting the actual joint position. By this, our error contains propagates inaccuracies in scaling the multibody dynamics model and thus reveals IMU-driven model personalization as a new challenge.
- The datasets are different. Besides walking, DIP-IMU and TotalCapture contain gestures, freestyle and range of motion movements. Therefore, there is no fair comparison between our method and PIP.

C Additional Results

Physics Finetuning and personalization of IMU positions: We list the visual (see Figure 4) results of the physics finetuning and quantitative

results (see Table 5) of the physics finetuning and IMU positioning personalization experiments. GRFs and joint torques are estimated more accurately, while the joint angles show slightly higher error.

Table 5: Quantitative comparison between the physics-finetuned model, personalized IMU orientations and rotation, and the baseline model.

IMU configuration	JAE	JTE	GRF	Jitter	Speed
Baseline	8.9	5.0	18.8	1.95	0.15
Physics Finetuned	9.3	4.5	14.9	1.15	0.20
Personalized	9.0	5.0	17.8	1.92	0.14

Ablations: To justify the importance of the individual loss terms and implementation details, we performed an ablation study. The results are shown in Table 6. The ablations are explained as follows: 1.) *w/o est-ankle*: We do not estimate ankle kinematics separately, we use the full-body kinematics to estimate the GRFs instead. 2.) *w/o input noise*: We remove the input noise from the IMU signals. 3.) *w/o GRF minimum*: We remove the minimum bound on the GRFs. 4.) *w/o \mathcal{L}_{FS}* : We remove the foot speed loss. 5.) *w/ two contact points*: Instead of defining a single contact point based on the global foot angle, we set a fixed contact points for the foot and the heel, respectively. This is similar to the ground contact model in [14].

We show that all ablations lead to a decrease in performance. We note that the GRF minimum is especially important because it prevents local minima where the model does not learn to interact with the ground.

SSPINNpose combined with PIP’s second stage: To combine PIP with SSPINNposes second stage, we first estimate the global kinematics with SSPINNpose and track the joint angles q and joint velocities \dot{p} with a PD controller. Instead of projecting contact polygons from contact points, we deviated from the original PIP implementation by using the heel and toe positions as the contact points. We heuristically set the ground contact probability as a function of the horizontal speed of the contact points and estimated GRFs. The PD controller was tuned manually ($k_\lambda = 0.01$, $k_{res} = 0.1$, $k_\tau = 0.1$).

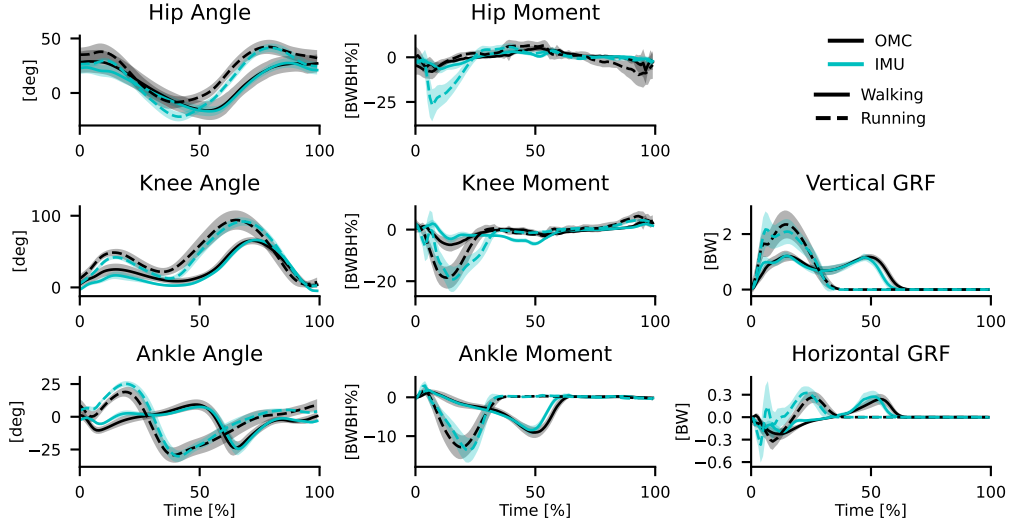


Figure 4: Average joint angles, torques and GRFs for the right leg, estimated with a physics-finetuned Bi-LSTM baseline model. We segmented the gait cycles during which the force plate was hit and normalized them to a duration of 100 samples. Walking and running data is shown in solid and dashed lines, respectively. Our estimations are shown in cyan, the reference data is shown in black. The shaded area represents the standard deviation.

Table 6: Quantitative results from the ablation study

Model Version	JAE	JTE	GRF	Jitter	Speed
Full	8.9	5.0	18.8	1.95	0.15
w/o est-ankle	9.4	4.7	27.1	3.59	0.20
w/o noise augmentation ($\eta_{imu} = 0$)	9.1	5.0	17.7	2.34	0.15
w/o GRF minimum	34.0	-	-	2.95	0.86
w/o \mathcal{L}_{FS}	9.7	5.4	19.3	2.25	0.18
w/ two contact points	12.8	4.7	21.6	2.05	0.30

Sparse IMU configurations: In Figure 5, we show the stick figures for the sparse IMU configurations. We show that the model is able to estimate physically and visually plausible motions for all configurations. The errors

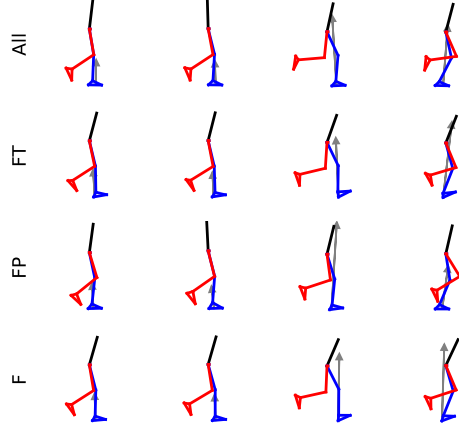


Figure 5: Sample stick figures for sparse IMU configurations, with forces annotated in gray. The rows show (from top to bottom) all IMUs, foot and thigh (FT) IMUs, and foot and pelvis (FP) IMUs, only foot (F) IMUs. We show random samples with the first two columns showing walking data, and the last two columns showing running data. All samples are drawn randomly from different participants.

are higher for the foot and thigh (FT) configuration, as the thigh IMUs are more prone to soft-tissue artefacts. The errors are lowest for the foot and pelvis (FP) configuration, as the pelvis IMU is less affected by soft-tissue artefacts.

Sensitivity to IMU misplacement: We retrained SSPINNpose with IMU positions that were perturbed by varying offsets in the sagittal plane. We did a training run each with offsets of 2 cm, 4 cm, 6 cm, 8 cm, 10 cm, 15 cm, and 20 cm in a random direction. Next, we tested whether SSPINNpose was able to recover either the IMU positions from the finetuning experiment in Section 4.2 or the IMU positions in the dataset. The results in Table 7 indicate that SSPINNpose is robust to small variations in IMU placement, but performance degrades with offsets of 10 cm or more. Manual IMU placement or measurement should usually be accurate within less than 10 cm, so we consider this a reasonable level of robustness. Recovering the IMU positions in the dataset is more challenging, but as long the model has been trained on reasonably accurate IMU positions, it can partially recover the IMU po-

sitions. This is shown by the optimized offsets compared to the finetuning experiment and dataset being smaller than the offsets used for training.

Table 7: Experiments regarding the sensitivity to IMU misplacement and recovery of IMU positions. The first four columns show the evaluation metrics when training with offset IMU positions. The last two columns show the offsets compared to the original finetuning experiment the IMU positions in the dataset (DS).

Offset cm	JAE [deg]	JTE [BWBH%]	GRF [BW%]	Speed [m s ⁻¹]	Offset vs. Sec. 4.2 cm	Offset vs. DS cm
Baseline	8.9	5.0	18.8	0.15	0.0 +- 0.0	4.7 +- 2.2
2	9.4	5.5	19.1	0.13	4.4 +- 2.0	2.2 +- 1.2
4	9.7	5.9	19.5	0.14	6.1 +- 2.5	4.3 +- 2.5
6	8.4	5.1	17.6	0.13	3.8 +- 2.3	2.1 +- 1.4
8	10.4	5.7	20.9	0.16	5.8 +- 2.3	4.1 +- 1.8
10	16.4	4.7	36.1	2.99	7.6 +- 3.3	6.3 +- 3.7
15	14.1	6.0	22.1	0.52	15.1 +- 8.7	14.5 +- 9.9
20	18.5	5.3	19.7	0.39	24.1 +- 11.6	23.7 +- 12.5

D Graphical Overview of SSPINNpose training and evaluation scheme

In Figure 6, we give an overview of the training and evaluation scheme of SSPINNpose. The explanation to the graphic is as follows: **A:** We take continuous IMU signals, body constants, IMU positions and ground contact model parameters as input. **B:** We use a (Bi-) LSTM to output kinematics and joint torques. **C:** We show a stick figure of the estimated kinematics at $\{2.5, 3.0, \dots, 4.5\}$ s. For two out of these frames, we also show the reference kinematics in grey. **D:** We supervise our model using the loss functions introduced in Section 3.2. Here we show: 1.) *Kane’s Loss*, which has the same dimensionality as the multibody dynamics model’s degrees of freedom. 2.) *Temporal Consistency Loss* for $\mathbf{p}_{ankle,r}$, where the estimated velocity is

shown in black and the estimated acceleration in red. The dashed lines represent the numerical differentiation of the position and velocity, respectively. 3.) *Virtual IMU*: The simulated IMU signals of a foot-worn IMU. 4.) *Foot-IMU speed*: The estimated speed of the foot-worn IMU, our model in blue and the kalman-filter based integration in green. The shaded area marks the zone where the speed error is zero. **E**: We show the biomechanical outcome variables. Dashed lines represent the reference data. 1.) *Kinematics*: Hip flexion: blue; knee flexion: red; ankle plantarflexion: green. 2.) *Speed*: Translational velocity. 3.) *Torques*: Knee flexion: red, ankle plantarflexion: green. The hip flexion torque is not shown as it is out of range, but it is not estimated correctly for this trial. 4.) *GRFs*: Vertical: blue, horizontal: red.

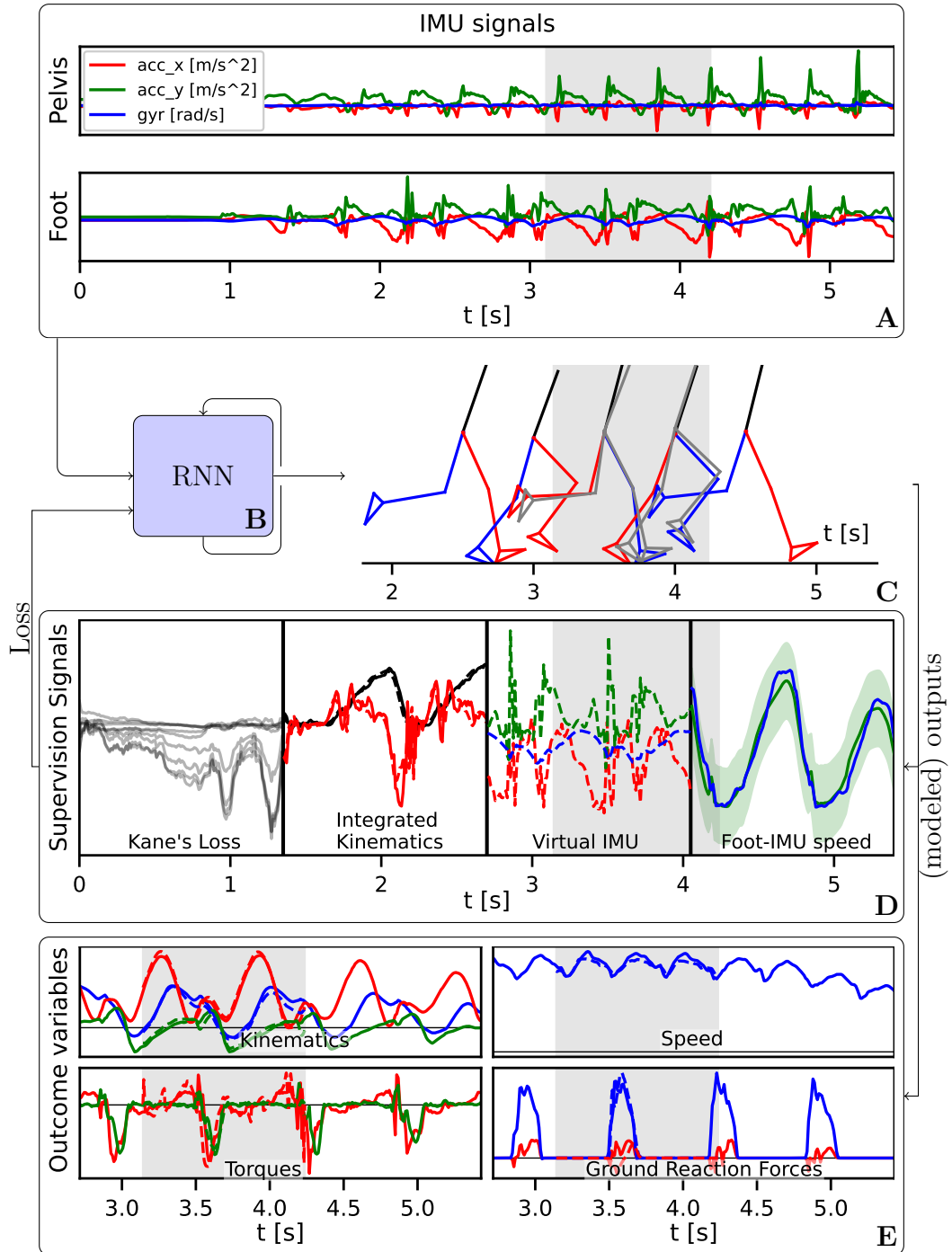


Figure 6: Overview of the SSPINNpose training and evaluation process. All data shown is from a single running bout at a max speed of 4.9 m s^{-1} . The shaded area marks the time where the reference data was recorded.